



ORIGINAL ARTICLE

CT-derived indices of canine osteosarcoma-affected antebrachial strength*

Tanya C. Garcia, MS¹ | Michele A. Steffey, DVM, Diplomate ACVS-SA²  | Allison L. Zwingenberger, DVM, Diplomate ACVR²  | Leticia Daniel, MV² | Susan M. Stover, DVM, PhD, Diplomate ACVS¹

¹Department of Anatomy, Physiology and Cell Biology Surgical, School of Veterinary Medicine, University of California—Davis, Davis, California

²Department of Radiological Sciences, School of Veterinary Medicine, University of California—Davis, Davis, California

Correspondence

Michele A. Steffey, Diplomate ACVS-SA, Department of Surgical and Radiological Sciences, School of Veterinary Medicine, University of California—Davis, 1 Shields Ave, Davis, CA 95616.
Email: masteffey@ucdavis.edu

Funding information

Center for Companion Animal Health, School of Veterinary Medicine, University of California—Davis

Abstract

Objective: To improve the prediction of fractures in dogs with bone tumors of the distal radius by identifying computed tomography (CT) indices that correlate with antebrachial bone strength and fracture location.

Study design: Prospective experimental study.

Animals: Dogs with antebrachial osteosarcoma (n = 10), and normal cadaver bones (n=9).

Methods: Antebrachia were imaged with quantitative CT prior to biomechanical testing to failure. CT indices of structural properties were compared to yield force and maximum force using Pearson correlation tests.

Results: Straight beam failure (Fs), axial rigidity, curved beam failure (Fc), and craniocaudal bending moment of inertia (MOICrCd) CT indices most highly correlated (0.77 > R > 0.57) with yield and maximum forces when iOSA-affected and control bones were included in the analysis. Considering only OSA-affected bones, Fs, Fc, and axial rigidity correlated highly (0.85 > R > 0.80) with maximum force. In affected bones, the location of minimum axial rigidity and maximum MOICrCd correlated highly (R > 0.85) with the actual fracture location.

Conclusions: CT-derived axial rigidity, Fs, and MOICrCd have strong linear relationships with yield and maximum force. These indices should be further evaluated prospectively in OSA-affected dogs that do, and do not, experience pathologic fracture.

1 | INTRODUCTION

Osteosarcoma (OSA) primarily affects the appendicular skeleton of large and giant breed dogs, particularly the distal radial metaphysis.¹ Treatment of OSA generally consists of surgical excision of the primary lesion followed by adjuvant chemotherapy. Amputation is the surgical procedure most commonly recommended for appendicular OSA excision¹

but the presence of other concurrent orthopedic or neurologic disease may preclude this option in some dogs. Surgical limb-salvage procedures for distal radial OSA in the dog provide survival times comparable to those with amputation. However, complications are common, especially infections, reported in up to 78% of cases.¹⁻⁸ Alternatively, radiation-based therapies have been described as an alternative for limb salvage in the veterinary literature, but do not alleviate the risks of pathologic fractures.^{4,9-12} In people, other in situ non-surgical therapies for the management of primary and metastatic appendicular bone neoplasia include thermal

*These data have been presented in part as a poster presentation at the American College of Veterinary Surgeons Annual Meeting, October 6-8, 2016, Seattle, WA.

ablation and selective arterial embolization.¹³ In situ treatment may offer benefits over surgical removal, such as potential inhibition of metastasis through a variety of mechanisms.¹⁴⁻¹⁹ As most dogs with OSA ultimately die of distant metastatic disease, in situ treatment could be especially relevant in this species, if metastasis inhibition is confirmed. However, these therapies are relatively unexplored in the dog, and the risk of pathologic fracture in tumor-affected bone must be considered before clinical application.

Previous work has described the fundamental biomechanics of canine antebrachia with tumor-invaded bone in dogs with distal radial OSA.¹⁵ Accurate determination of the risk of pathologic fractures in individual canine patients with OSA would allow evidence-based recommendations for candidates to limb salvage. At this time, no criteria have been established to determine the risk of pathologic fracture in veterinary patients. Prediction of pathologic fracture in people with primary or metastatic bone neoplasia has been evolving. Radiographic measurements (DEXA) have limited ability to predict femur fractures in people.^{16,17} Estimates of 3-dimensional (3D) geometry and density from 2-dimensional (2D) radiographs are based on assumptions of a symmetric bone and a homogeneous density in each cross-section. These assumptions are compounded by technical control issues, such as low resolution and influence of rotational position of the bone. Engineering beam theory can be used to account for the material properties of bone tissue and the 3D geometry of the bone structure, and estimate axial and bending rigidities of whole bones.¹⁷⁻²² Estimates correlated well with measured failure force in human femurs.²⁰ Several in vitro studies have demonstrated that bone architecture, measured by computed tomography (CT), is a determinant of bone strength and has been found to improve pathologic fracture prediction in humans.^{19,23-25} CT determination of subchondral bone involvement in dogs with appendicular OSA is associated with time to fracture.²⁶ If structural properties derived from CT correlate with mechanical properties of OSA diseased bones, CT-derived indices may help evaluate the risk of fracture in clinical patients.

The aims of this study were to determine correlations between bone strength and site of fracture previously measured in vitro¹⁵ with corresponding CT-derived indices of bone strength. We hypothesized that at least 1 CT-derived index would correlate with the yield and failure strengths of neoplastic bones, as well as site of fracture.

2 | MATERIALS AND METHODS

2.1 | Study design

The study included 2 groups: (1) OSA affected unilateral forelimbs from 10 client-owned dogs (32-64 kg, 4-12 years old) that presented for treatment of unilateral primary OSA

of the antebrachium, and (2) unilateral forelimbs from 9 dogs (21-35 kg, unknown age in all except 2 dogs, both aged 12 years) euthanatized for reasons other than forelimb musculoskeletal pathology. Antebrachia were imaged using CT for subsequent determination of structural geometric properties and bone tissue densities. CT-derived indices were compared to mechanical testing variables determined from a previous study¹⁵ to determine the strength of correlations between structural properties based on in vivo CT imaging and actual failure strength.

This study was approved by the Institutional Animal Care and Use Committee, and informed owner consent was obtained prior to inclusion. Amputated tumor bearing limbs were obtained from 10 clinical patients with a solitary primary OSA of the antebrachium that was visible radiographically and confirmed using cytology or histopathology. Control limbs were obtained from 9 large breed canine cadavers without known orthopedic disorders. Limbs were stored at -20°C in sealed watertight bags.

2.2 | Imaging

CT scans of tumor-affected and contralateral unaffected limbs of 10 clinical tumor patients were performed under general anesthesia, and of a single limb from control cadavers ex vivo. Axial CT (LightSpeed 16, GE Medical Systems) was performed with the long axis of each limb aligned along the axial dimension of the gantry at 120 kVp and 200 mA at a resolution of 0.625 mm slice thickness and 0.406 mm pixels (512×512 pixel matrix). Images were reconstructed using a BONE convolution kernel. A Cann-Genant phantom (CT Calibration Phantom, Mindways Software Inc, San Francisco, California) with 5 known hydroxyapatite densities was placed in the field of view. In the clinical patients, the head was positioned out of the scan field of view to prevent attenuation artifacts.

Antebrachia were loaded axially to failure as previously reported.¹⁵ The measured structural properties compared to CT-indices were Yield and Maximum Forces and Energies because these variables are descriptors of structural yield and failure, and work to yield and failure. Yield Force captures initiation of permanent deformation in the bone structure and can promote failure under repetitive loading that occurs in vivo. Maximum force captures the force that induces complete failure. Pre-yield and post-yield energies capture the work required to achieve yield and maximum forces.

Digital radiographs (lateromedial [LM] and craniocaudal [CrCd] views) were taken before and after structural tests to characterize the geometry and location of bone failure (48 kVp, 4.6 mAs, Minxray HF 100/30+ generator and Sound-Eklin EDR3 digital control panel).

2.3 | Characterization of fracture type and location

The fracture location and proximal and distal margins of the OSA in affected antebrachia were measured as percentage of bone length from the distal end of the radius using calibrated LM radiographs. Bone length was measured from the cranial-to-caudal mid-point of the distal aspect of the radius to the center of rotation of the trochlear notch of the ulna. The type of failure was categorized as oblique, comminuted, transverse, or transverse and crushed.

2.4 | CT data reduction and relation to structural properties

Structural properties were calculated from CT image data using custom software (Matlab R2013b, Mathworks, Natick, Massachusetts). Images were rotated as necessary to achieve uniform anatomical alignment within the coordinate axes of the software. Mineralized bone was isolated from background and soft-tissue by thresholding at 300 Hounsfield units (HU). Mineralized bone pixel densities were converted from HU to hydroxyapatite concentrations using a linear relationship between calibration phantom hydroxyapatite concentrations and HU outputs.

Because structural properties are related to dog weight, and dog weight was unknown for 4 of 21 specimens, estimates of bone size and volume were assessed as potential surrogates for dog weight. Mid-diaphyseal cross-sectional area (CSA) was measured using CT data from a single mid-diaphyseal slice. Bone volume was estimated using 2 methods. The first method considered the bones' cross-sectional shape as an ellipse and used mid-diaphyseal width and depth measurements from LM and CrCd radiographs to calculate elliptical volume (V_e) where

$$V_e = \left(\frac{\text{LM Width}}{2} \right) * \left(\frac{\text{CrCd Depth}}{2} \right) * \pi * \text{Bone Length.}$$

The second method calculated bone volume (V_{csa}) where

$$V_{\text{csa}} = \text{CSA} * \text{Bone Length.}$$

The best estimate of bone volume was determined by assessing correlations between CSA, V_e , and V_{csa} with dog weight for dogs of known weight. The best correlation was used to estimate dog weight for the 4 dogs with unknown weights.

CT-derived indices of failure strength were based on the assumption that the antebrachium would fracture at either the weakest location along the length of the bone, and/or at the point of highest local stress due to a combination of loading, bone geometry, and material properties. Calculations based on engineering beam theory used CT data to estimate the value and location of the weakest transverse slice within the

CT volume. Because the antebrachium has a structure that approximates a mildly curved beam with mineral density heterogeneity and an architecture and geometry that are markedly altered by OSA, several indices were explored to find the best correlation with failure strength.

The first 2 indices calculated from CT data were the minimum axial (Min EA) and bending (Min EI) structural rigidities because of their relationship to fracture in previous studies.¹⁷⁻²² Structural rigidities were estimated for each CT slice by weighting the CSA [mm^2] and CrCd bending moment of inertia (MOI) [mm^4] of each pixel by the density dependent relationship for elastic moduli (E) [GPa], then summing the modulus-weighted rigidity of each pixel about the centroid or neutral axis as in the following equations.

$$\text{Axial Rigidity : } EA = \sum E_i dA$$

$$\text{Bending Rigidity : } EI = \sum E_i y_i^2 dA$$

where i is each pixel in the cross section, dA is pixel area, y is the CrCd distance of each pixel from the centroid, and \sum is the sum for all pixels in the CT cross section. Pixel moduli (E) were derived using a best-fit function relating previously reported experimentally observed bone mineral density (BMD) (mgHA/cc) and E . The data used were from a range of species, anatomic sites, and techniques for measuring modulus and mineral density as reported by Easley et al.²⁷ Data derived from human trabecular bone affected with metastatic neoplastic disease²⁸ were added to the data set because it was expected that OSA-affected bone would have similar properties to the lower BMD and E of trabecular bone with neoplasia. The resulting best-fit equation was $E = 1.34e-4 \cdot \text{BMD}^{1.7198}$.

The third and fourth indices, maximum (Max MOI) and minimum moment of inertia (Min MOI) were calculated as the CrCd bending MOI in each cross section using the equation:

$$\text{Moment of Inertia : } \text{MOI}_{\text{CrCd}} = \sum y_i^2 dA$$

The Min MOI and rigidities have been used to describe the weakest part of the bone.²² The Max MOI was analyzed because an increase in bone diameter appears to be a rapid, proliferative, poorly mineralized, woven bone response to neoplasia and associated osteolysis, which could be structurally weak.

The fifth index (Min Fs) is the minimum value of a calculated failure force for axial loading of an initially slightly curved beam, which results in a combination of axial compressive and bending loads, as derived by Lee et al.²⁰ The assumption of slight curvature means the bending moment is solely induced by the eccentric load axis relative to the bone centroid as illustrated in Figure 1. The general equation for stress is $\sigma = (F_s/A + Mc/I)$ where F_s is the critical (failure)

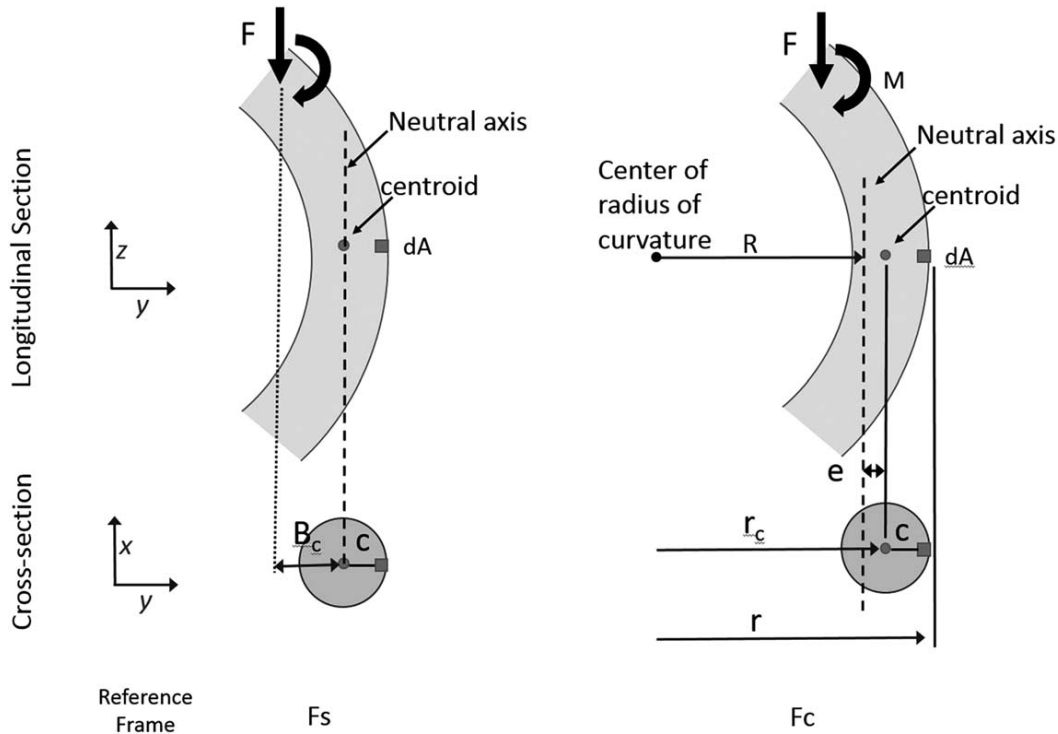


FIGURE 1 Schematic representation of indices used to calculate the predicted critical force for loading of the antebrachium modeled as a “slightly curved” beam (F_s) or a curved beam (F_c)

force, A is CSA, and I is MOI. Writing the equation in terms of strain (ϵ , where $\epsilon = \text{yield tensile bone strain} = 0.8\%^{29}$) using the relation $\sigma = E \cdot \epsilon$, the bending moment $M_c = F_s \cdot B_c$ where B_c is defined by the horizontal distance (resultant vector) from the axial compressive load axis to the centroid of the bone (c) which is the distance from the centroid to the outer extent of the bone in cross-section. Assuming a circular cross-sectional shape and solving for F_s the equation becomes:

$$\text{Slightly Curved Beam Critical Force} \\ : F_s = \frac{\epsilon}{\left[\left(\frac{1}{EA} \right) + \left(B_c \cdot \frac{c}{EI} \right) \right]}$$

The sixth index (Min F_c) is the minimum value of a calculation of the failure force for an initially curved beam loaded by a combination of axial compressive and bending loads. The assumption of a highly-curved beam takes into account the radius of bone curvature. The equation for stress is $\sigma = F_c/A + My/Ae(R-y)$ where F_c is the critical (failure) force.³⁰ Writing the equation in terms of strain (ϵ , where $\epsilon = 0.8\%^{29}$) using the relation $\sigma = E \cdot \epsilon$, and the indices shown in Figure 1 where $y = R - r$ where $R = \text{CSA} / \int dA/r$ (the radius of curvature to the neutral axis), and r is radius of curvature to the local point of interest (dA) on the bone. We assume the location dA is on the tensile side of the bone at the point furthest from the center of the radius of curvature (ie, cranial), due to the natural curvature of the bone. The bone's cross-section is approximated by a circle to estimate the radius of curvature to the neutral axis, $R = 1/2(r_c + \sqrt{r_c^2 - c^2})$ where

$r_c = \text{radius of curvature to the centroid}$ (determined by fitting a parabola to the path of the centroid along the bone at each cross-section using the equation $r_c = [1 + (dz/dy)^2]^{3/2} / d^2z/dy^2$, where dz/dy and d^2z/dy^2 are the first and second derivatives, respectively, of the parabolic equation), $c = \sqrt{A/\pi}$, which is the distance from the centroid to the outer extent of the bone in cross-section assuming a circular cross-sectional shape and $e = r_c - R$; and solving for F_c the equation becomes:

$$\text{Curved Beam Critical Force} : F_c = \frac{\epsilon}{\left[\left(\frac{1}{EA} \right) + \left(\frac{r_c \cdot y}{EAe \cdot (R - y)} \right) \right]}$$

The seventh index (Min F_b) assumes that failure was due to the minimum critical force of buckling of an intermediate column. Buckling is the mode of failure due to axial compressive load on a beam or column with a CSA relatively small compared to its length. Buckling failure is due to a high local stress creating lateral motion (failure of) local material followed by loss of structural compressive support and subsequent bending. F_b is defined below, where L is the length of the tested bone (unconstrained bone length, that is, proximal bone not in potting material to distal end).³¹

$$\text{Buckling Critical Force} : F_b = \frac{\pi^2 EI}{L^2}$$

An eighth index (Max B_c) was a simple index to only capture bone curvature. B_c is defined by the horizontal cranio-caudal distance (resultant vector) from the axial

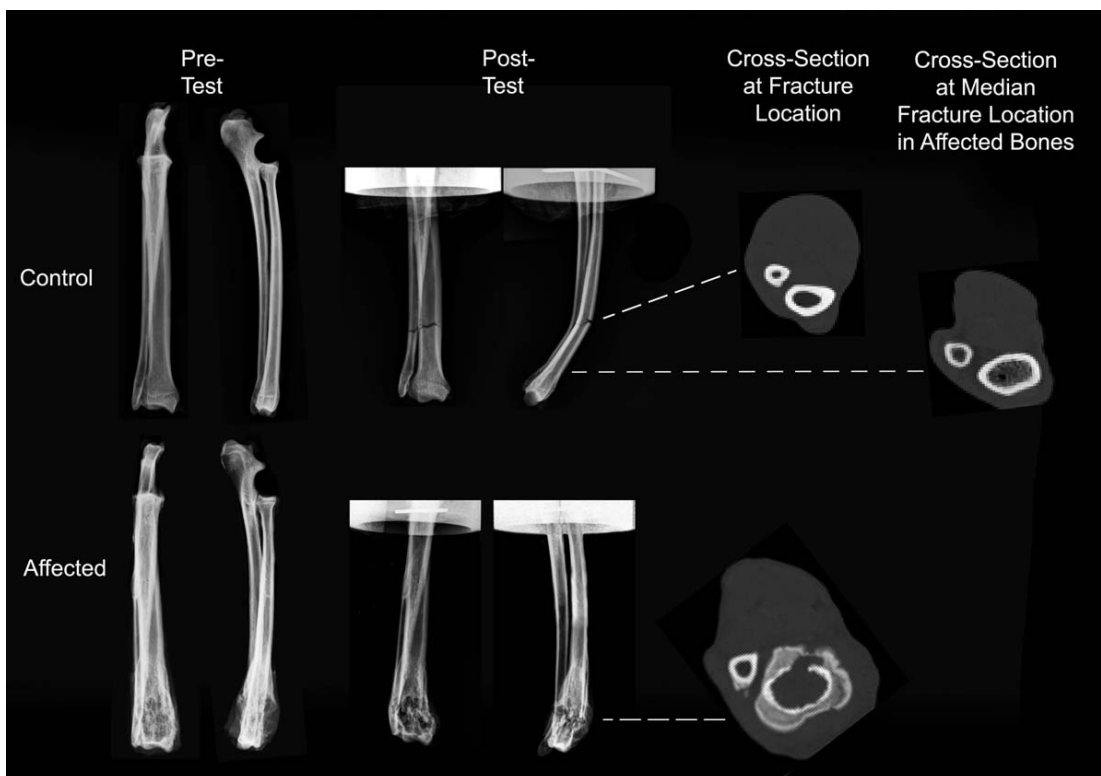


FIGURE 2 Radiographs representative of pre-test and post-test fracture location in OSA-affected and unaffected control bones. Cross-sections of the bones were obtained at the fracture site. A cross-section of the control bone taken from the median location of the fracture in OSA-affected bones is also shown

compressive load axis to the centroid of the bone at each CT slice. The maximum value was used presuming this location would have the highest tensile strain in bending.

Bone Curvature : $B_c = \text{Distance from load axis to centroid}$

The location of the slice within the CT volume that corresponded to each failure index is reported as a percent of the bone's length from the distal end.

2.5 | Statistical analysis

The Pearson correlation statistic was used to identify the bone size or volume measure that most highly correlated to the known dog body weights. Because CSA had the highest correlation ($R^2 = 0.89$, $P = < .001$) with the known dog body weights, the linear relation between CSA and body weight was used to estimate the 4 unknown body weights.

Three steps were used to determine which of the 8 CT-derived indices best correlated with previously determined bone strength variables (Yield and Maximum Forces, and Pre-Yield and Post-Yield Energies). First, a Principal Component analysis (proc PrinComp, SAS 9.3, SAS Institute, Cary, North Carolina) was used to determine if there were significant correlations between any linear combination of the CT indices and a second linear combinations of the mechanical properties. Six of the 8 CT-derived indices had

the largest principal components and were included in the following multiple correlation analysis (Canonical correlation, proc CanCorr) to examine the relationships between linear combinations of the CT-derived indices with the 4 bone strength variables. The Canonical correlation resulted in higher correlations between Yield Force and Maximum Force with the CT-derived indices than did pre-yield energy and post-yield energy. Therefore, Pearson correlations (proc Corr) assessed the individual relationships between the 6 CT-derived indices with Yield Force and Maximum Force.

Pearson correlations were also used to investigate whether the location (CT slice) of the minimum or maximum CT-derived index correlated with the location of the antebrachial fracture. Because the location and type of fracture were qualitatively different in affected bones compared to control bones, additional correlations for only affected bones and only control bones were analyzed separately.

3 | RESULTS

3.1 | Body-weight surrogate

Bone mid-diaphyseal CT-derived CSA had the highest correlation with 15 known dog body weights (r value = 0.89, P value = $< .001$, $CSA = 1.422 \cdot \text{body weight} + 16.5$). V_c and

V_{csa} had strong correlations but less than the correlation with CSA ($r = 0.76$ and $r = 0.84$, respectively).

3.2 | OSA location

The OSA extended to the distal end of the antebrachia in all affected bones (Figure 2) except 1, which extended distally to 15.7% of the bone length. The proximal extent of the OSA in affected antebrachia was $31.7\% \pm 10.2\%$ (mean \pm standard deviation) of bone length.

3.3 | Failure type and location

The OSA-affected antebrachia fracture location occurred at $19.7\% \pm 15.0\%$ of bone length from the distal end. One affected bone had an oblique radial fracture at the proximal-most portion of the OSA. One affected bone fractured proximal to the OSA (at 55.9% bone length). This bone was harvested from the youngest dog in the study (4 years old) and was the only one to sustain a comminuted fracture. All other affected bones fractured transversely on the cranial aspect and obliquely on the caudal aspect, consistent with tensile and compressive components due to bending. All bent bones also seemed crushed at the OSA fracture site (Figure 2). The ulna in all OSA-affected bones fractured at the same fracture location as the radii. All 9 normal antebrachia failed via transverse radial fracture on the cranial aspect and oblique on the caudal aspect. This configuration was consistent with bending where the oblique component directed proximocranial to distocaudal; 2 of these were comminuted (Figure 2). The fractures were located at $34.5\% \pm 3.3\%$ of the bone length. The ulnar fractured in only 6 of the 9 control antebrachial, at $21.0\% \pm 6.9\%$ bone length, distally to the corresponding radial fracture in 5 specimens. The 3 ulna that did not fracture were displaced from the radius.

3.4 | Correlation between CT-derived indices and mechanical properties

The correlations between CT and mechanical force data from affected and unaffected control bones were analyzed together and separately because affected antebrachia seemed to differ in morphology, fracture configuration, and because OSA and control groups had separate clusters on correlation scatter plots. Min Fs, Min EA, Min Fc, Max MOI_{CrCd} , and Min EI correlated to forces ($0.76 \geq R \geq 0.46$, $P < .05$) when all bones were grouped (Table 1). Min EA, Min Fc, Min Fs, Max MOI_{CrCd} , and Min EI also correlated to forces ($0.84 \geq R \geq 0.65$, $P < .05$) when considering only OSA-affected bones. Based on control bones only, Min Fs, Min EI, and Max MOI_{CrCd} correlated to forces ($0.84 \geq R \geq 0.67$, $P < .05$) (Table 1).

The linear relationships between the 4 CT-predicted indices that correlated best with yield and maximum forces are

TABLE 1 Significant ($P < .05$) correlation coefficients between CT-derived indices and yield and maximum mechanical test forces^a

CT-derived Index	Correlation coefficient (R)	
	Yield force	Maximum force
<i>Affected and control bones</i>		
Min Fs	0.71	0.76
Min EA	0.67	0.69
Min Fc	0.56	0.58
Max MOI_{CrCd}	0.59	0.57
Min EI	0.46	0.52
<i>Affected bones</i>		
Min EA	0.80	0.84
Min Fc	0.78	0.80
Min Fs	0.72	0.80
Max MOI_{CrCd}	0.73	0.69
Min EI	0.65	0.71
<i>Control bones</i>		
Min Fs	0.84	0.78
Min EI	0.72	0.67
Max MOI_{CrCd}	0.75	NS

^aMin EA is axial rigidity, Min EI is bending rigidity, Min Fs is the minimum predicted failure force in a slightly curved beam model, Min Fc is the minimum predicted failure force in a curved beam model, Max MOI_{CrCd} is the maximum cranio-caudal moment of inertia, Max Bc is the maximum cranio-caudal distance of the centroid to the line of axial force applied.

illustrated in Figures 3 and 4. When all bones tested in the study were considered, Min Fs achieved a relationship close to 1:1 with the yield force and maximum force (slope of the best fit linear equation is 1.1 and 1.2, respectively). When the analysis was limited to OSA-affected bones, Min Fs also has a close relationship with yield force and maximum force (slope of 1.04 and 1.15, respectively), whereas Min Fc under predicts the yield force and maximum force (slope of 0.009 and 0.009, respectively).

Control bones fractured at a location between 30% and 41% of the bone length from the distal end of the bone, seemingly unrelated to the location of Min or Max CT-derived indices. OSA affected bones fractured in the location of the OSA, that is, between 8% and 32% of bone length, with 1 exception in a young dog, where the fracture occurred proximal to the OSA at 56% bone length. Therefore, the correlation of the location of the CT-indices to fracture location was analyzed with and without this potential outlier (Table 2). When all bones in the study were combined, the location of the Max MOI_{CrCd} , Max Bc, and Min EA correlated ($0.61 \geq R \geq 0.52$, $P < .05$) with the location of the actual fracture location (Table 2). When OSA-affected bones were evaluated, Max MOI_{CrCd} , Min Fs, and Min EA correlated ($0.97 \geq R \geq 0.85$, $P < .05$) with fracture location and the slope of the relationship is 1.7, 0.26, and 0.58, respectively

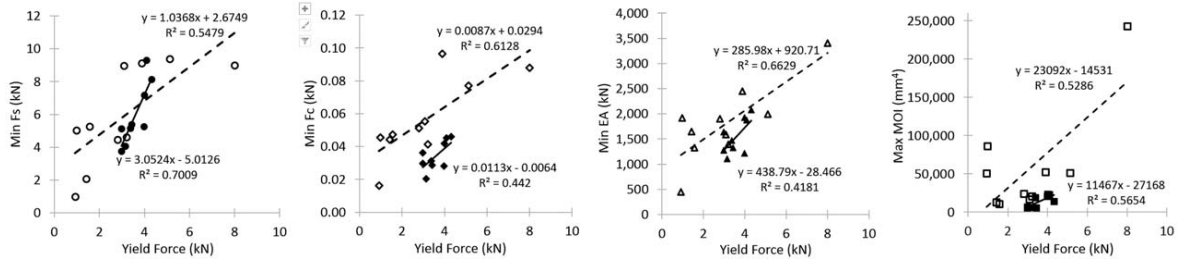


FIGURE 3 Plots representing the linear relationship between CT-predicted indices and yield force in OSA-affected (open markers) and unaffected control (filled markers) bones. The equation for the least-squares linear fit are shown for OSA-affected (dashed line) and unaffected control (solid line) bones

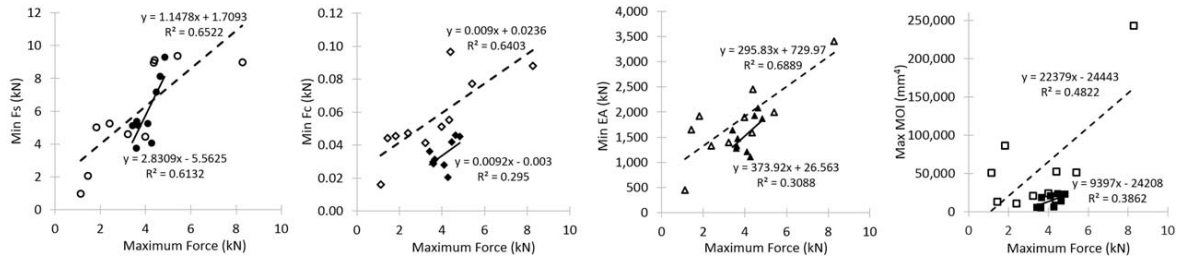


FIGURE 4 Plots representing the linear relationship between CT-predicted indices and maximum force in OSA-affected (open markers) and unaffected control (filled markers) bones. The equation for the least-squares linear fit are shown for OSA-affected (dashed line) and unaffected control (solid line) bones

(Figure 5). If the potential outlier is eliminated, Min Fs and Max MOI_{CrCd} strongly correlated ($R \geq 0.90$, $P < .05$) with fracture location (slope of the relationship is 1.3 and 1.2, respectively) (Figure 6). In control bones, no correlation was

identified between CT indices locations and actual fracture location ($R < 0.21$, $P > .05$).

4 | DISCUSSION

Four CT-derived indices correlated strongly with yield and maximum forces and fracture location in OSA-affected bones: Min EA, Min Fc, Min Fs, and Max MOI_{CrCd}. All affected bones with 1 exception failed at the OSA site, in the distal portion of the antebraechium. Two CT indices, Min Fs and Max MOI_{CrCd}, closely predicted the site of fracture in OSA-affected antebraechia, but not in unaffected control antebraechia.

The correlation between Max MOI_{CrCd} and fracture location and ultimate force in OSA-affected bones reflects the ability of this measurement to capture the geometry of the rapid, proliferative, poorly mineralized bone, which could be structurally weak. Max MOI_{CrCd} correlates weakly to ultimate force in normal bones, and does not correlate with Fracture Location in these controls because these specimens have a normal mineralization and homogenous structure. Under these conditions, Max MOI_{CrCd} should be the most resistant to failure.

Min EA may have a strong relationship to ultimate force and Fracture Location in OSA-affected bones because of the weakness created in less mineralized bone (sum of the density per cross-section), within the OSA lesion. In this group, Min EI had a low correlation to ultimate force because forces

TABLE 2 Significant ($P < .05$) correlations between the location of the respective Min or Max of the CT-derived indices and the location (% of bone length from the distal end of the radius) of fracture from mechanical tests^a

CT-derived location	Correlation coefficient (R) Fracture location
<i>Affected and control bones</i>	
Max MOI _{CrCd}	0.61
Max Bc	0.61
Min EA	0.59
Min Fc	0.52
<i>Affected bones</i>	
Max MOI _{CrCd}	0.97
Min EA	0.85
Min Fc	0.72
<i>Affected bones, outlier removed</i>	
Min Fs	0.93
Max MOI _{CrCd}	0.90

^aFor the “affected bones, outlier removed” section, the OSA-affected bone that did not fracture within the region of the tumor was removed from the analysis. See Table 1 for definition of abbreviations.

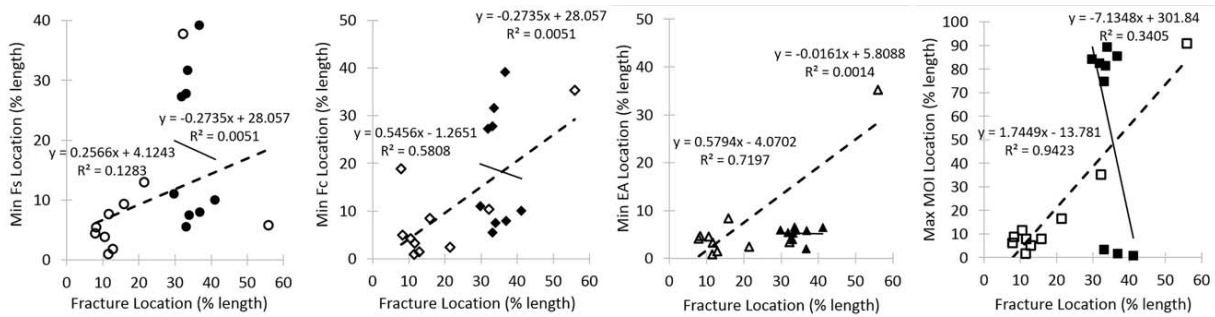


FIGURE 5 Plots representing the linear relationship between location of the CT-predicted indices and fracture location in OSA-affected bones (open markers) and unaffected control (filled markers) bones. The equation for the least-squares linear fit are shown for OSA-affected (dashed line) and unaffected control (solid line) bones

generated through axial loading were mainly compressive, given the shape and width of the neoplastic bone. Conversely, Min EA did not correlate with force at failure in control bones, whereas such correlation was identified for Min EI. This finding is likely due to the curvature of bones increasing bending forces relative to compression, when bones are loaded axially.

The strongest correlation between CT-derived parameters and biomechanical properties involved Min Fs, with a nearly a 1:1 relation with affected bone yield force and a strong correlation with fracture location. The relationship between Min Fs and force can be explained because this parameter combines geometric and mineral-density properties, using an equation adjusted to a long structure subjected to axial and bending loading. The equation used to calculate Fc assumes a highly-curved beam and uses radius of curvature to define distances (such as moment arm in bending). Since Min Fc correlated more weakly to force or fracture location than Fs (straight beam), modeling these bones antebrachia (affected or not) as straight beams seems more appropriate than modeling them as highly curved beams.

The greater variation in CT-derived indices observed in OSA-affected antebrachia compared to control antebrachia could be useful in assessing the risk of fracture in OSA-affected dogs. The lowest values for MinFs, MinFc, or

MinEA were measured in 2 dogs with OSA and corresponded to lower antebrachial yield and failure forces than those of all control dogs. Although the 2 neoplastic bones had not sustained a pathologic fracture prior to the current study, these antebrachia could have been predisposed to fracture. These findings warrant a prospective comparison between CT-derived indices of dogs with pathologic fractures secondary to OSA and those of dogs with antebrachial OSA that do not fracture.

Study limitations are related to the *in vitro* biomechanical study that provided the yield and failure force data, and availability of specimens. We have previously reported that the *in vitro* loading conditions used here did not simulate all *in vivo* loading modes or cyclic loading conditions.¹⁵ However, these loading conditions did simulate the most common loading circumstance during stance in dogs. The age of dogs enrolled in the control group was largely unknown. Since age affects bone density and mechanical properties, the influence of this parameter on the antebrachial mechanical properties in this study could not be determined. However, most of the CT-derived indices (except MaxMOI) accounted for bone density and/or bone geometry, which are the main factors impacting the mechanical properties of bone. Our findings could be considered as proof-of-concept for application to other appendicular bones affected with OSA. However,

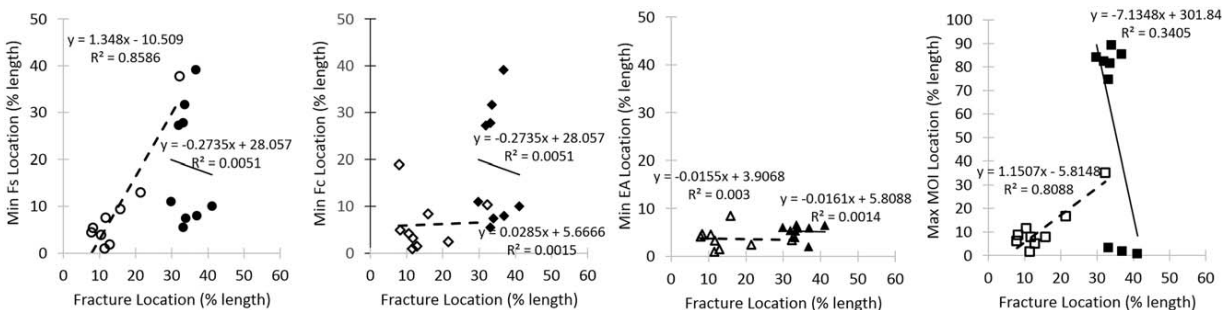


FIGURE 6 Plots representing the linear relationship between location of the CT-predicted indices and fracture location in OSA-affected bones (open markers), after exclusion of the young dog whose bone fractured outside the osteosarcoma site, and unaffected control (filled markers) bones. The equation for the least-squares linear fit are shown for OSA-affected (dashed line) and unaffected control (solid line) bones

such application would require that CT-derived indices be determined for each bone. The threshold for fracture may also be site-dependent, as OSA in distal radial sites may be less prone to pathologic fractures than other appendicular bone tumors in dogs.³²

The CT-based indices Min Fc, Min EA, and Min Fs have strong linear relationships to yield and maximum forces and fracture location in vitro. These parameters may therefore be useful to identify OSA-dogs at low risk for pathologic fracture. To verify which of the indices truly predict pathologic fracture, CT-derived indices should be prospectively compared between dogs with pathologic fractures secondary to OSA and dogs with antebrachial OSA that do not fracture. The results of the current study laid the groundwork for future investigation in this area.

ACKNOWLEDGMENTS

The authors are grateful to Richard Larson for invaluable technical assistance in conducting this study. The described project was supported with funding from the Center for Companion Animal Health, School of Veterinary Medicine, University of California—Davis.

CONFLICT OF INTEREST

The authors have no conflicts of interest to disclose.

REFERENCES

- [1] Withrow SJ, Page R, Vail DM. *Withrow and MacEwen's Small Animal Clinical Oncology*. 5th ed. St. Louis, MO: Elsevier; 2013.
- [2] Mitchell KE, Boston SE, Kung M, et al. Outcomes of limb-sparing surgery using two generations of metal endoprosthesis in 45 dogs with distal radial osteosarcoma. A Veterinary Society of Surgical Oncology retrospective study. *Vet Surg*. 2016;45:36-43.
- [3] Liptak JM, Dernell WS, Ehrhart N, et al. Cortical allograft and endoprosthesis for limb-sparing surgery in dogs with distal radial osteosarcoma: a prospective clinical comparison of two different limb-sparing techniques. *Vet Surg*. 2006;35:518-533.
- [4] Liptak JM, Dernell WS, Lascelles BD, et al. Intraoperative extracorporeal irradiation for limb sparing in 13 dogs. *Vet Surg*. 2004;33:446-456.
- [5] Liptak JM, Dernell WS, Straw RC, et al. Intercalary bone grafts for joint and limb preservation in 17 dogs with high-grade malignant tumors of the diaphysis. *Vet Surg*. 2004;33:457-467.
- [6] Morello E, Vasconi E, Martano M, et al. Pasteurized tumoral autograft and adjuvant chemotherapy for the treatment of canine distal radial osteosarcoma: 13 cases. *Vet Surg*. 2004;32:539-544.
- [7] Seguin B, Walsh PJ, Mason DR, et al. Use of an ipsilateral vascularized ulnar transposition autograft for limb-sparing surgery of the distal radius in dogs: an anatomic and clinical study. *Vet Surg*. 2003;32:69-79.
- [8] Ehrhart N. Longitudinal bone transport for treatment of primary bone tumors in dogs: technique description and outcome in 9 dogs. *Vet Surg*. 2005;34:24-34.
- [9] Boston SE, Duerr F, Bacon N, et al. Intraoperative radiation for limb sparing of the distal aspect of the radius without transcarpal plating in five dogs. *Vet Surg*. 2007;36:314-323.
- [10] Farese JP, Milner R, Thompson MS, et al. Stereotactic radiosurgery for treatment of osteosarcomas involving the distal portions of the limbs in dogs. *J Am Vet Med Assoc*. 2004;225:1567-1572.
- [11] Walter CU, Dernell WS, LaRue SM, et al. Curative-intent radiation therapy as a treatment modality for appendicular and axial osteosarcoma: a preliminary retrospective evaluation of 14 dogs with the disease. *Vet Comp Oncol*. 2005;3:1-7.
- [12] Covey JL, Farese JP, Bacon NJ, et al. Stereotactic radiosurgery and fracture fixation in 6 dogs with appendicular osteosarcoma. *Vet Surg*. 2014;43:174-181.
- [13] Mavrogenis AF, Rossi G, Rimondi E, et al. Palliative embolization for osteosarcoma. *Eur J Orthop Surg Traumatol*. 2014;24:1351-1356.
- [14] Joosten JJ, Muijen GN, Wobbles T, et al. In vivo destruction of tumor tissue by cryoablation can induce inhibition of secondary tumor growth: an experimental study. *Cryobiology*. 2001;42:49-58.
- [15] Steffey MA, Garcia TC, Daniel L, Zwingenberger AL, Stover SM. Mechanical properties of canine osteosarcoma-affected antebrachii. *Vet Surg*. 2017;doi:10.1111/vsu.12628.
- [16] Beck TJ, Ruff CB, Warden KE, et al. Predicting femoral neck strength from bone mineral data. A structural approach. *Invest Radiol*. 1990;25:6-18.
- [17] Snyder BD, Hauser-Kara DA, Hipp JA, et al. Predicting fracture through benign skeletal lesions with quantitative computed tomography. *J Bone Joint Surg Am*. 2006;88:55-70.
- [18] Snyder SM, Schneider E. Estimation of mechanical properties of cortical bone by computed tomography. *J Orthop Res*. 1991;9:422-431.
- [19] Hong J, Cabe GD, Tedrow JR, et al. Failure of trabecular bone with simulated lytic defects can be predicted non-invasively by structural analysis. *J Orthop Res*. 2004;22:479-486.
- [20] Lee T. Predicting failure load of the femur with simulated osteolytic defects using noninvasive imaging technique in a simplified load case. *Ann Biomed Eng*. 2007;35:642-650.
- [21] Whealan KM, Kwak SD, Tedrow JR, et al. Noninvasive imaging predicts failure load of the spine with simulated osteolytic defects. *J Bone Joint Surg Am*. 2000;82:1240-1251.
- [22] Smith MD, Baldassarri S, Anez-Bustillos L, et al. Assessment of axial bone rigidity in rats with metabolic diseases using CT-based structural rigidity analysis. *Bone Joint Res*. 2012;1:13-19.
- [23] Bauer JS, Link TM. Advances in osteoporosis imaging. *Eur J Radiol*. 2009;71:440-449.
- [24] Tanck E, van Aken JB, van der Linden YM, et al. Pathological fracture prediction in patients with metastatic lesions can be improved with quantitative computed tomography based computer models. *Bone*. 2009;45:777-783.
- [25] Hipp JA, Springfield DS, Hayes WC. Predicting pathologic fracture risk in the management of metastatic bone defects. *Clin Orthop Relat Res*. 1995;312:120-135.
- [26] Kubicek L, Vanderhart D, Wirth K, et al. Association between computed tomographic characteristics and fractures following

- stereotactic radiosurgery in dogs with appendicular osteosarcoma. *Vet Radiol Ultrasound*. 2016;57:321-330.
- [27] Easley SK, Jekir MG, Burghardt AJ, et al. Contribution of the intraspecimen variations in tissue mineralization to PTH- and raloxifene-induced changes in stiffness of rat vertebrae. *Bone*. 2010;46:1162-1169.
- [28] Kaneko TS, Bell JS, Pejcic MR, et al. Mechanical properties, density and quantitative CT scan data of trabecular bone with and without metastases. *J Biomech*. 2004;37:523-530.
- [29] Keaveny TM, Wachtel EF, Ford CM, et al. Differences between the tensile and compressive strengths of bovine tibial trabecular bone depend on modulus. *J Biomech*. 1994;27:1137-1146.
- [30] Dowling NE. *Mechanical Behavior Of Materials: Engineering Methods for Deformation, Fracture and Fatigue*. 2nd ed. Upper Saddle River, NJ: Prentice Hall; 1999.
- [31] Vable M, ed. Stability of columns. *Mechanics of Materials*. 2nd ed., Vol. Online. New York: Oxford University Press; 2002.
- [32] Rubin JA, Suran JN, Brown DC, et al. Factors associated with pathological fractures in dogs with appendicular primary bone neoplasia: 84 cases (2007-2013). *J Am Vet Med Assoc*. 2015; 247:917-923.

How to cite this article: Garcia TC, Steffey MA, Zwingenberger AL, Daniel L, Stover SM. CT-derived indices of canine osteosarcoma-affected antebrachial strength*. *Veterinary Surgery*. 2017;00:1-10. <https://doi.org/10.1111/vsu.12645>